Water liquid distribution in a bioinspired PEM fuel cell

Alfredo Iranzo [a,], G.M. Cabello González [a], Baltasar Toharias [a], Pierre Boillat [b], Felipe Rosa [a]*

[a] *Departamento de Ingeniería Energética, Grupo de Termotecnia. Escuela Técnica Superior de Ingeniería. Universidad de Sevilla. Camino de Los Descubrimientos s/n. 41092 Sevilla Spain*
[b] *Electrochemistry Laboratory and Neutron Imaging and Activation Group, Paul Scherrer Institute, Switzerland*

HIGHLIGHTS

- Neutron imaging study of the water distribution in a 50 cm² bioinspired PEM cell.
- Effect of operating temperature, pressure, current density, and humidity is discussed.
- Water accumulates preferentially in the anode side as a consequence of permeation.

ARTICLE INFO

ABSTRACT

Water management is a key factor in the operation of hydrogen fuel cells since its formation may lead to significant mass transport losses, oxygen diffusion limitation and membrane durability issues. In this work, the effect of different operating conditions on the liquid water distribution inside a 50 cm² active area bio-inspired PEM fuel cell has been studied. Therefore, a set of experiments was designed varying cell pressure, the reactants relative humidity (anode and cathode), temperature, and cell current density. Liquid water distribution for each operating condition was determined using neutron imaging technique as it has been proved to be an excellent technique for this purpose, including quantitative analysis and water profiles in the different areas of the bio-inspired flow field. The results show that high relative humidity of the inlet gas flows, high pressure, low temperatures and low current density favor the accumulation of water in the flow field channels and GDL. Specifically, water accumulates preferentially in the anode side that make contact with the low part of the cathode foams inserted in the flow field, instead of blocking the closest area to the gases outlets points. This is due to permeation from the cathode foams to the anode side.

1. Introduction

The latest road-maps released by economic powers such as United States [1,2] and Europe [3] to achieve a carbon-free society points to hydrogen as a main sustainable energy vector, where fuel cells are regarded as sustainable energy conversion devices transforming hydrogen into electric energy, and generating only water as by-product. That way, fuel cells have proven to be a more environmental-friendly technology

compared to current energy conversion systems, provided that hydrogen is obtained from renewable sources [4]. Nowadays, Polymer Electrolyte Membrane fuel cells (PEMFC) are commercially present not only for stationary purposes, but also for mobility applications [5] such as an alternative to internal combustion engines because it is a clean technology with zero emissions, relatively simple layout and greater efficiency [6]. However, as fuel cells are composed out of various components whose interaction impacts the cell functionality, there is still room for improvement in order to accelerate their widespread, increasing their performance, lifetime, and minimizing their fabrication and operational costs, not only of the single fuel cell or stack [7], but also of the whole hybrid system where the fuel cell is integrated [8]. In that sense, understanding the fundamentals of PEM fuel cells is crucial to reach optimal designs that break the last barriers to the technology implementation.

Throughout the fuel cell operation, water is produced at the cathode due to the oxygen reduction reaction (ORR). Also, water is transported from the anode to the cathode via electro-osmotic drag, potentially resulting in the dehydration of the anode. At higher power, PEM fuel cells generate a considerable amount of water that, due to the operating condition required by the membrane ($60-90\,°C$ and $1-2$ bar), is partly found in a liquid state and can result in the accumulation of water excess flooding the cell [7]. This flooding effect not only blocks the pores used by oxygen to reach the catalyst layer, but also decreases catalytic sites in the membrane for the electrochemical reaction to occur [9]. On the other hand, polymer electrolyte membranes need to absorb a certain amount of water in order to preserve their ionic conductivity. That way, water management in PEM fuel cells is thus one of the most important and active research topics being addressed in order to achieve higher power densities in stacks for final applications. Most of the literature found about water and also heat management make use of novel tools such as three-dimensional multi-phase computational fluid dynamics to model and optimize PEM fuel cell designs [10], but fewer experimental studies can be found due to the difficulty of observing the inside of the cell. In this sense, a Computational Fluid Dynamics model was developed by Andersson et al. [11] to study water transport in a channel relevant to Proton Exchange Membrane Fuel Cells (PEMFCs). The model employs a volume of fluid approach and incorporates experimental validation using synchrotron-based X-ray imaging. The results demonstrate good agreement between the model and measurements, revealing the influence of channel height on droplet behavior and the impact of the gas diffusion layer's contact angle on droplet size. The research of Iranzo et al. [12] introduces a modeling framework for simulating diffusive mass transport limitations in PEM fuel cells at a local scale, with a specific focus on the distribution of liquid water in the porous media. By incorporating experimental measurements obtained through neutron imaging, the framework maps the liquid water distribution into the simulation model, allowing for a more accurate representation. This approach enhances the coupling of experimental measurements and model development, resulting in more reliable models for understanding fuel cell phenomena. Zhao et al. [13] took in-situ measurement using micro-sensors in the cathode flow field

plate under different conditions. Their work proves that the relative humidity has a great effect on the internal resistance of PEM fuel cells as high temperatures or low gas humidity leads to membrane dry out. On the other hand, higher gas humidity and higher pressure can alleviate this problem, but may also result in cathode channel flooding. PEM fuel cells thus depends on an optimum water management to reach their most effective performance and extend the life-span of the membrane. The design of bipolar plates among with the operating condition tuning is a key aspect in order to get a proper water management, avoiding flooding and improving cell operation, especially at high current densities [14].

Among other techniques such as X-ray [15] or magnetic resonance, neutron imaging has been proved to be an excellent method to evaluate the water content in fuel cells [16—18], stimulating in a successful way the understanding and optimization of PEM fuel cells. It makes use of neutrons as radiation for the image acquisition process, being the resulting images mostly radiographs that represent the intensity of the neutrons transmitted through a sample, providing the water distribution in devices working under realistic operating conditions [19—21]. Making use of this technique, previous research in water management in commercial serpentine bipolar plates showed that, as expected, the presence of liquid water in the cathode rises as the relative humidity of the inlet gases, both anode and cathode gases, grow [17]. The anode relative humidity had much less influence than the cathode relative humidity in the fuel operation. Also, high humidity had a positive impact on the fuel cell performance as the water content in the MEA causes a decrease in the ohmic resistance at low current density. Besides, the cell was found drier at higher current densities because of the large gas flows and cell temperature. As well, the accumulated water decreases as the cathode stoichiometry increases because a higher cathode flow has a better ability to remove water [22].

Bipolar plates design plays an important role in water management since gas flow channel scheme and dimensions significantly affect water accumulation [23]. Biomimetics take inspiration from nature and is based on the designs that evolution has optimized over the centuries to technological spearhead applications. That way, bipolar plates for polymer electrolyte membrane fuel cells could be optimized to reach a better performance of the fuel cell. In fact, in the later years there has been an upsurge of studies of nature-inspired [24] (lungs, leaves, sponges, honeycomb shape) bipolar plates that have proven to present higher performance, improved water management, lower pressure drops and provide more homogeneous gas distributions [25—30]. Kang et al. [31] investigated leaf designs for bipolar plates mimicking ginkgo and dicotyledonous leaves. They found that none of their design overcame the maximum power density or water removal capacity reached for the commercial serpentine although both leaf designs improved the parallel pattern design. Nasu et al. [32] studied water management in a comb-shaped cathode serpentine anode cell. They observed that gas stream velocity was a key parameter for removing liquid water and that, at low current densities, liquid water was found in the gas inlet whereas at high current densities, it moves towards the outflow gas channels. The use of a hydrophobic GDL results in water spreading more uniformly in the anode channels what

indicates that the water generated at the cathode is diffused to the anode side. Also, the heat generated by the cathode overvoltage leads to a low water condensation at the cathode and anode, reducing the ohmic overvoltage and suppressing the increase in diffusion overvoltage. In the field of design and simulation, Asadzade et al. [33] have investigated the more common flow patterns to get a uniform pressure, velocity and reactant distribution through the surface of the catalyst layer and design a lung-inspired pattern for a bipolar plate. Their simulation showed that the developed pattern improved the cell performance, as it presented less pressure loss, a much uniform reactant distribution and suitable fluid velocity. Trogadas et al. have a background in the research of nature-inspired solutions for fuel cells. They have developed a lung inspired flow field that distributes reactants in a uniform way [34,35]. Their design presents two regions, an upper one with a branch pattern and a lower one with clusters of acini. They observed in a commercial serpentine that in the anode water started to accumulate in the corners of the channels while in the cathode spread across the surface of the channel in the direction of the flow. Their lung inspired design favored the aggrupation of water drop and therefore the cell flooding even at low current densities [36]. However, once they installed a thin graphite plate with capillaries, water accumulation occurred only on the anode side while the water generated at the cathode was quickly removed from the channels, decreasing pressure drop and increasing power density a 30% when compared with the commercial serpentine design [37]. Suárez et al. [38] have also presented a study in the line of bioinspired PEM fuel cells. Four designs were selected taking as a starting point a CFD fluid flow analysis of different configurations. Then, experimental results indicated that one of the proposed biomimetic design is particularly suited for improving water management at high reactants humidity reaching out a peak power a 6.0% higher in comparison with the reference commercial serpentine design. Future research should, therefore, analyze water distribution within the channels of this novel design.

According to Jiao et al. [39] there are two established design approaches for bipolar plate structural designs, involving modifications to the channel-rib structure or the development of flow fields with micro-baffles or porous structures. Graphene's unique combination of properties makes it an attractive material for including porous structures in PEM fuel cells, as it offers exceptional electrical conductivity, a large surface area, a lightweight and porous structure, chemical stability, corrosion resistance, and effectiveness in water management. Its high electrical conductivity facilitates efficient electron transfer, while its large surface area enhances electrochemical reactions and catalyst-reactant contact. The lightweight and porous structure allows for efficient gas transport and effective water management. Additionally, graphene's chemical stability and corrosion resistance ensure long-term stability of fuel cell components. In terms of water repellency, graphene generally exhibits a hydrophobic behavior, with reported contact angles ranging from around 80 to over 95° [40,41]. Graphene foam has been reported to improve PEM fuel cell performance and they are the logic evolution of the innovative metal foam. Several studies such as the one carried out by Kumar et al. [42], Wang et al. [43] or

Tseng et al. [44] proposed the use of metal foam as the flow field for bipolar plates in order to create a convective and diffusive gas flow pathway, reaching an enhanced heat management and electron transport due to the high thermal and electrical conductivity of the metal foams, preventing water flooding and improving performance. However, metal foams are susceptible to corrosion and the use of metal components in MEAs can lead to contamination by metal ions. Chen et al. [45] introduced graphene foam, a three-dimensional material created by depositing graphene onto nickel foam and removing the nickel using chemical wet-etching. This material combines the advantages of metal foams with graphene's unique properties, eliminating corrosion concerns. When used as a flow field in PEM fuel cells, they achieved uniform reactant distribution and prevented water flooding. Park et al. [46] proved that a graphene-foam flow field improved mass transport and higher performance at high current densities based on single-cell tests. Analysis of oxygen gain, electrochemical impedance spectra, and simulations indicated that a graphene-foam MEA exhibited lower mass-transport resistance compared to a conventional MEA [47]. This advantage stems from graphene foam's ability to facilitate the efficient mass transport of reactants and water.

This paper provides a deeper insight into the fuel cell water management in order to find how the operating conditions (cell pressure, the reactants relative humidity (anode and cathode), temperature and cell current density) affect the liquid water distribution inside the bipolar plates channels of a bio-based design. The design of filling the cathode channels of the cell with a graphene mimics the structure and function of natural systems such as the structure of the lung alveoli, which are tiny air sacs in the lungs that allow for efficient gas exchange. The alveoli have a complex three-dimensional structure that is composed of thin walls and a network of small channels that allow for the interchange of gases between the air and the bloodstream. Similarly, the graphene foam acts as a porous structure that allows for efficient transport of oxygen to the cathode, where the oxygen reduction reaction takes place. Graphene porous sponges and lungs demonstrate similarities in their structure and functionality. They both possess a porous nature, with graphene porous sponges constructed from interconnected graphene sheets and lungs composed of an intricate network of air sacs and passages. This porous composition enables a substantial surface area, which plays a crucial role in facilitating efficient gas diffusion and exchange, having high gas permeability. Additionally, both structures possess a notable surface area-to-volume ratio, promoting enhanced gas exchange efficiency by providing ample space for gas molecules to interact. The insertion of graphene foam in a fuel cell can also be compared to the structure of a plant's vascular system, specifically the xylem. The xylem is a network of tiny tubes that transport water and nutrients from the roots to the leaves of a plant. Similarly, the porous structure of graphene foam can act as a network of tiny tubes that transport gases within the fuel cell. Moreover, the hierarchical structure of xylem, from the microscale to the macroscale, provides efficient transport and distribution of fluids and nutrients throughout the plant. Similarly, the hierarchical structure of graphene foam, with interconnected pores at multiple length scales, can provide

efficient network for transport and distribution of fluids and gases.

Neutron imaging was used over a 50 cm^2 PEM fuel cell to determine the liquid water distribution at each operating condition in both, flow field channels (cathode and anode) and gas diffusion layers. The main novelty of the study is the application of neutron imaging to investigate the liquid water distributions in a bio-inspired fuel cell for a comprehensive set of operating conditions. To the best of the authors' knowledge, there is not such a complete analysis of water distribution in a bioinspired cell design using neutron imaging to assess a set of different operating conditions.

2.   Experimental facility and methodology

2.1.   Cell description

All the experiments have been carried out making use of a bio-inspired graphite 50 cm^2 active area cell fuel. The design of the cell has been carried out by Suárez et al. [38] and it comprises a cathode with an inlet and outlet collector connected in parallel with 6 groups of straight channels in sets of 7 channels each. Six derivations from the inlet collector and the outlet collector were considered (one for each group) simulating the branching distributions of the bronchi in the outermost part of the lungs. A bio-inspired modification of this concept was made inserting in the central part of the vertical channels of each of the six groups for graphene porous sponge inserts (density of 320 mg/cm^3 and pore size of 580 μm) from Graphene Supermarket (Ronkonkoma, NY, USA). A detailed image of the design can be found in Ref. [38]. The most fundamental point is that the complete flow field is inspired by lungs, and not only the porous foam. The main horizontal feed channel for the inlet gas on top of the flow field would be corresponding to the windpipe, and the set of short vertical channels connecting the main feed channel with the porous foams would be corresponding to the bronchi. Thus, the porous foam is designed to resemble the alveoli within the lungs bulk volume. The anode, on the other hand, is a commercial graphite serpentine flow field from ElectroChem Inc. That way, the flow field layout is cross flow, circulating the gases in the cathode vertically and in the anode horizontally.

The membrane electrode assembly used during the tests is a GORE® PRIMEA® MEAs A510.1/M665.15/C580.4 with a platinum loading of 0.1 mg/cm^2 at the anode side, 0.4 mg/cm^2 at the cathode side and 15 μm thick. Also, a set of Freudenberg H23C6 gas diffusion layer of 250 μm thick were assembled.

2.2.   Experimental procedure

A comprehensive set of experiments was carried out (Table 1) in order to study how the different operating conditions affect water distribution in the cell. The studied variables were anode-cathode relative humidity, temperature, pressure and current density. For all tests, anode and cathode stoichiometry was 1.3 and 2.5 respectively. Also, relative humidity was kept symmetric i.e. same value in cathode and anode side (RH$_{a,c}$) for each test.

Neutron imaging experiments, presented in Table 1, were carried out as described in Iranzo et al. [22] at the SINQ-NEUTRA beam-line at Paul Scherrer Institut, Villigen (Switzerland) [29,30] with a 10 s exposure time. Previous to every test, the cell was dried out circulating dry nitrogen through anode and cathode. The cell was operated in galvanostatic mode setting the current, and anode-cathode flows at each operating condition. In order to remove the water accumulated during one test to have a fresh start in the next one, liquid water was flushed by sudden decompression of the anode and cathode in a short time so the GDL and the MEA hydration were not significantly affected [18,48,49]. The images obtained through this procedure enable the differentiation of liquid water distribution both in the channels of the bipolar plate and in the gas diffusion layers.

Once the images were taken, the radiographs were corrected and referenced pixel-wise by dividing the attained images by a dry cell image, so the attenuation corresponding only to water is obtained. The water thickness is calculated making use of the Lambert-Beer law [17].

3.   Results and discussion

This section presents the results of the neutron imaging tests carried out with the biomimetic design and the main conclusions regarding the water accumulation and management are exposed. The effect of changing the operating conditions in the liquid water distribution is assessed, to determine which parameters affects water management the most. Finally, a detailed analysis of the water accumulation in some particular areas of the cell allows to draw and study the water accumulation profiles in the anode and cathode separately.

3.1.   Effect of the operating conditions

Images resulting from neutron radiographies are presented below (Figs. 2–4) where the gas inlets are on the top left and the outlets on the bottom right of the figures. In the yellow-blue images, blue color corresponds to the amount of liquid water deposited, corresponding the shaded blues to water in GDL and dark blue lines to water accumulated in the channels. It can clearly be seen that there are significant differences in the liquid water detected in the cell depending on the different operating conditions. When reporting the results, three differentiated zones have been considered (Fig. 1), each one corresponding to different structures in the cathode flow field: gas inlet, corresponding to the reagent access zone, comprising the area occupied by the vertical cathode access channels (~10 cm^2); middle part, corresponding to the area occupied by the cathode foams (~30 cm^2); and gas outlet zone, which includes the area occupied by the vertical and horizontal gas outlet channels of the cathode (~10 cm^2). It must be considered that the reported value of liquid water in each zone corresponds to the sum of both anode and cathode contributions. It can however be observed that liquid water is found in both cathode (vertical channels with a wide foam space in the image) and anode (serpentine horizontal channels) and that it tends to accumulate in the outlet region of the flow field (lower part of the images). This occurs because the

Test	RH$_{a,c}$ (%)	T (ºC)	P (bar,g)	F$_a$ (NmL/min)	F$_c$ (NmL/min)	CD (A/cm^2)	Cathode feed
1	60	65	0.5	444	2032	1	air
2	90	65	0.5	444	2032	1	air
3	60	65	1	444	2032	1	air
4	90	65	1	444	2032	1	air
5	60	65	0.5	222	1016	0.5	air
6	90	65	0.5	222	1016	0.5	air
7	60	65	1	222	1016	0.5	air
8	90	65	1	222	1016	0.5	air
9	60	70	0.5	222	1016	0.5	air
10	60	55	0.5	222	1016	0.5	air

Table 1 – Operating conditions defined for the set of experiments (RH$_{a,c}$ is the relative humidity on anode and cathode, T stands for temperature, P for pressure, F$_a$ and F$_c$ is the gas flow in anode and cathode respectively and, CD is the current density).

gas gradually becomes saturated with water in vapor phase as it flows through the channels until water condensates, flooding the channels and limiting gas diffusion, influencing in a negative way the cell performance.

3.1.1. Effect of pressure

Experiments 1 and 3 (Table 1) have been carried out at the same operating conditions except for the pressure, which rises from 0.5 to 1 bar. It can clearly be seen that the amount of water in the channels of both anode and cathode increases as the pressure does (Fig. 2). The same happens at a higher relative humidity as it is shown in experiments 2 and 4, where even the inlet cathode channels present a considerable amount of liquid water. The same tendency can be spotted at higher current density (Fig. 3). It can be seen that the section that increase the most its water content is the foam section followed by the inlet section, whereas the inlet zone is almost unaltered. For example, focusing in experiments 1 and 3, water content rises 0.63 g in total, increasing 0.13 g the outlet section, 0.49 g the foam section and 0.01 g the inlet section. This makes sense since the foam section is the largest one and therefore has a higher liquid water retention capability. On the other hand, if the amount of water per area is considered, the most affected section is the outlet zone (an increase of 0.0262 g/cm^2 average in the outlet zone vs 0.0001 g/cm^2 average in the foam zone) since gases are progressively saturated along their route through the channels of the cell. As the gas outlet is situated in the lower part of the cell, gravity also contribute to this preferential accumulation.

3.1.2. Effect of anode and cathode relative humidity

Anode and cathode relative humidity dramatically impacts the presence of water in the fuel cell. In Figs. 2 and 3, it can be seen that for both operating pressures (0.5 and 1 bar) at high and low current density (1 and 0.5 A/cm^2), the amount of liquid water flooding the flow field rises as the inlet gases humidity does, especially in the foam (an increase of 0.4 g of water and 0.0033 g/cm^2 average for each of the four pairs of experiments) but, above all, in the outlet zone of the cell (an increase of 0.0075 g of water and 0.040 g/cm^2 average for each of the four pairs of experiments). In this case, though, a significant amount of liquid water appears in the inlet section for the tests with a 90% of anode/cathode relative humidity (an increase of 0.1 g of water average for each of the four pairs of experiments). This early appearance of condensed water in the channels of the fuel cell is due to the fact that the reactant streams are very close to saturation, so the slightest generation of water causes complete saturation of the gas stream, which leads to a higher rate of water condensation.

3.1.3. Effect of temperature

In experiments 5, 9 and 10 (Table 1), temperature is varied from the highest value (70 °C) to the lowest one (55 °C). As
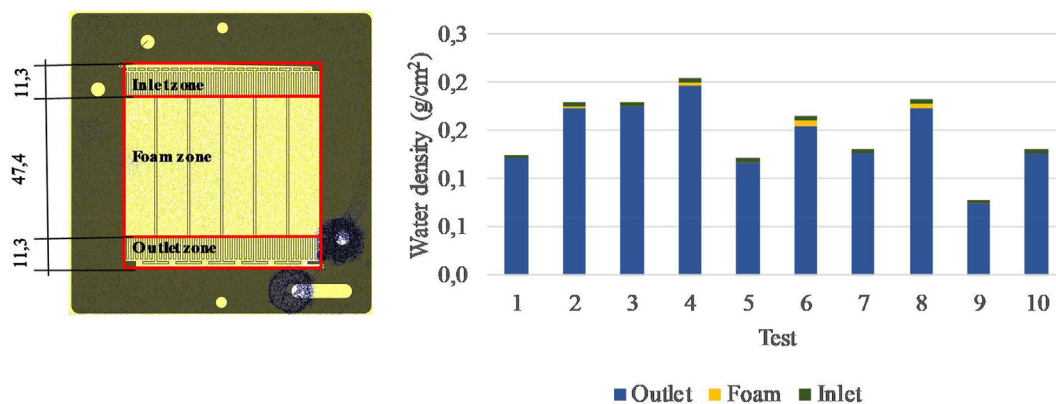

Fig. 1 – Amount of water per surface on each one of the selected zones for the tests listed in Table 1. Dimensions of the zones length in mm.
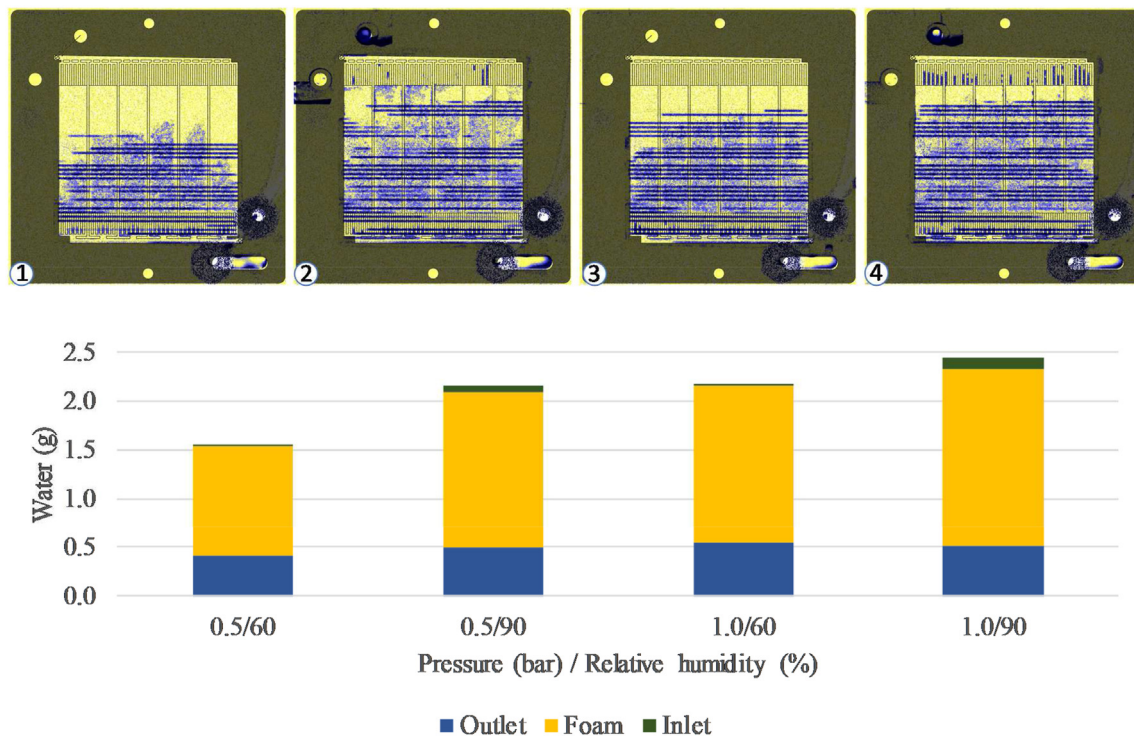
Fig. 2 — Effect of relative humidity and pressure on water distribution (T = 65 °C, CD = 1 A/cm²). Liquid water distribution in the cell from neutron radiographies of the experiments 1, 2, 3 and 4 listed in Table 1 (top), and amount of water in the cell (bottom).
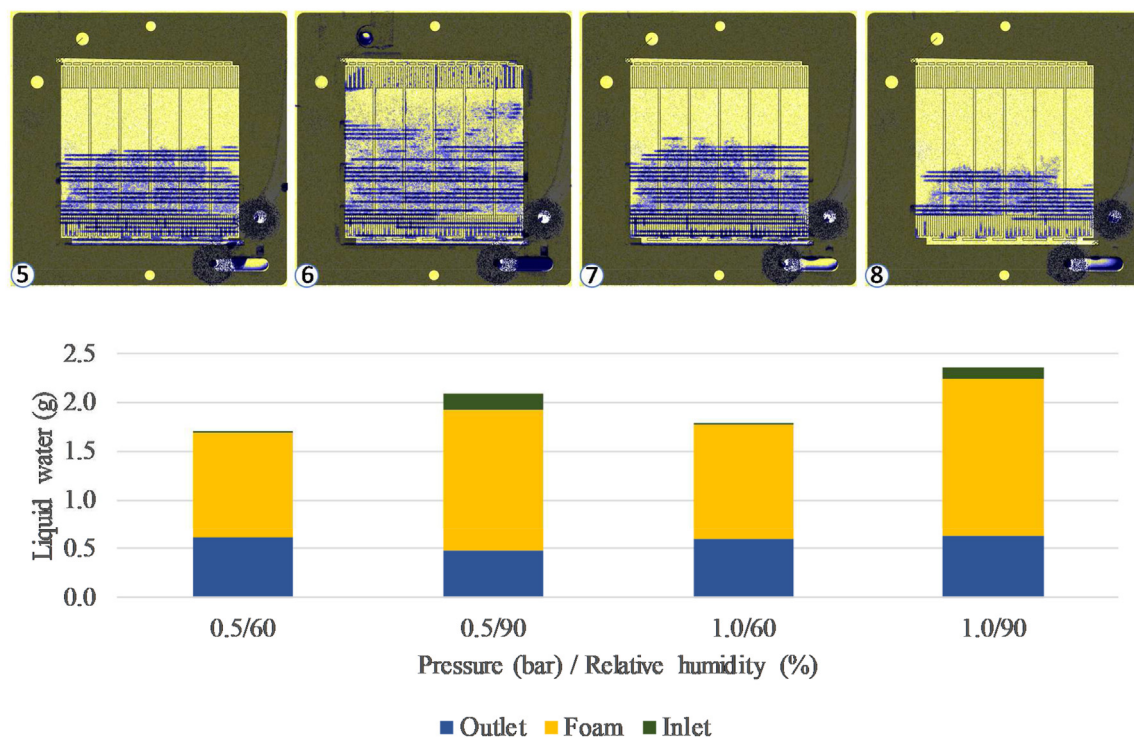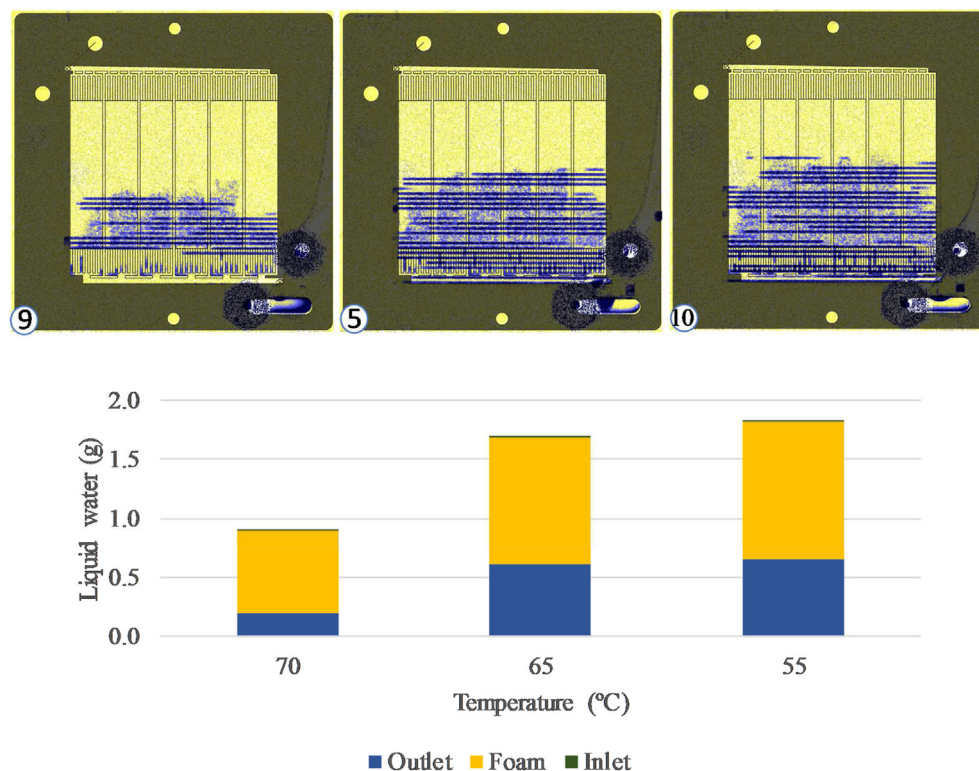

Fig. 3 — Effect of relative humidity and pressure on water distribution (T = 65 °C, CD = 0.5 A/cm²). Liquid water distribution in the cell from neutron radiographies of the experiments 5, 6, 7 and 8 listed in Table 1 (top), and amount of water in the cell (bottom).

Fig. 4 — Effect of temperature on water distribution. Liquid water distribution in the cell from neutron radiographies of the experiments 7, 8 and 9 listed in Table 1 (top), and amount of water in the cell (bottom).

expected, as the temperature decreases, the amount of water accumulated in the flow fields and GDLs increases due to the loss of the ability of the gas to accept water in the vapor phase (Fig. 4). This increase in the presence of liquid water as temperature decreases is not linear, rather, the amount of water detected is greater in the interval between 70 and 65 °C (an increase of 0.8 g) than in the interval between 65 and 55 °C (an increase of 0.13 g).

3.1.4. Effect of current density

The effect of current density in liquid water distribution in the cell can be observed in Figs. 5 and 4. Experiments 1 and 5 present the same operating condition except for the current density, that is higher in experiment 1 (1.0 vs 0.5 A/cm^2). The same occurs between experiments 2 and 6, but this pair shows a higher relative humidity (90% vs 60%). As before applies for the pair of tests 3 and 7, and 4 and 8 in Fig. 6. According to Faraday's law, a higher water production occurs at higher intensities, however, the gas flow in the anode and cathode flow field is also higher at this operating condition, facilitating water removal and preventing flooding. In addition, at higher current densities the local temperature at the MEA is increasing due to the heat generation and this is contributing to the evaporation of liquid water. A rise in the amount of liquid water as current density increases is shown in Fig. 4 between experiments 3 and 7, and 4 and 8 (increase of 0.39 and 0.08 g respectively). On the other hand, at lower pressures for the smaller relative humidity (Fig. 5), the presence of water is diminished (a decrease of 0.16 g) as current density rises. At

high relative humidities this effect is less significant since the cell is already almost flooded.

The work of Suárez et al. [38] provides a detailed comparison of the performance between the lung-inspired model and a conventional serpentine design for the operating conditions studied. Although the biomimetic design exhibited lower performance compared to the 5-channels parallel-serpentine design at lower cell temperatures (4% lower), higher cell backpressure (6% lower), and a higher cathode stoichiometric factor (21% lower), the novel biomimetic design demonstrated superior performance at higher relative humidity (RH) values of 90%. It achieved a peak power output that was 6% higher, indicating that the design is suitable for improved water management under conditions of high reactant humidity.

3.2. Analysis of water accumulation profiles

In order to analyze the specific distribution of water within the bio-based bipolar plate design, two different experiments from the design have been considered in order to analyze the water distribution profiles in detail: test 9, with a low amount of water, and test 10, with a greater amount of liquid water accumulated. Water accumulation profiles have been presented along a set of significant lines, which are depicted in Fig. 7. Firstly, three lines have been chosen that run vertically along the central rib of the cathode (3) and those at both sides (1 and 5). In this way the water content within the cathode flow field is isolated, and the profiles are presenting only the water accumulated in the anode side. On the other hand,
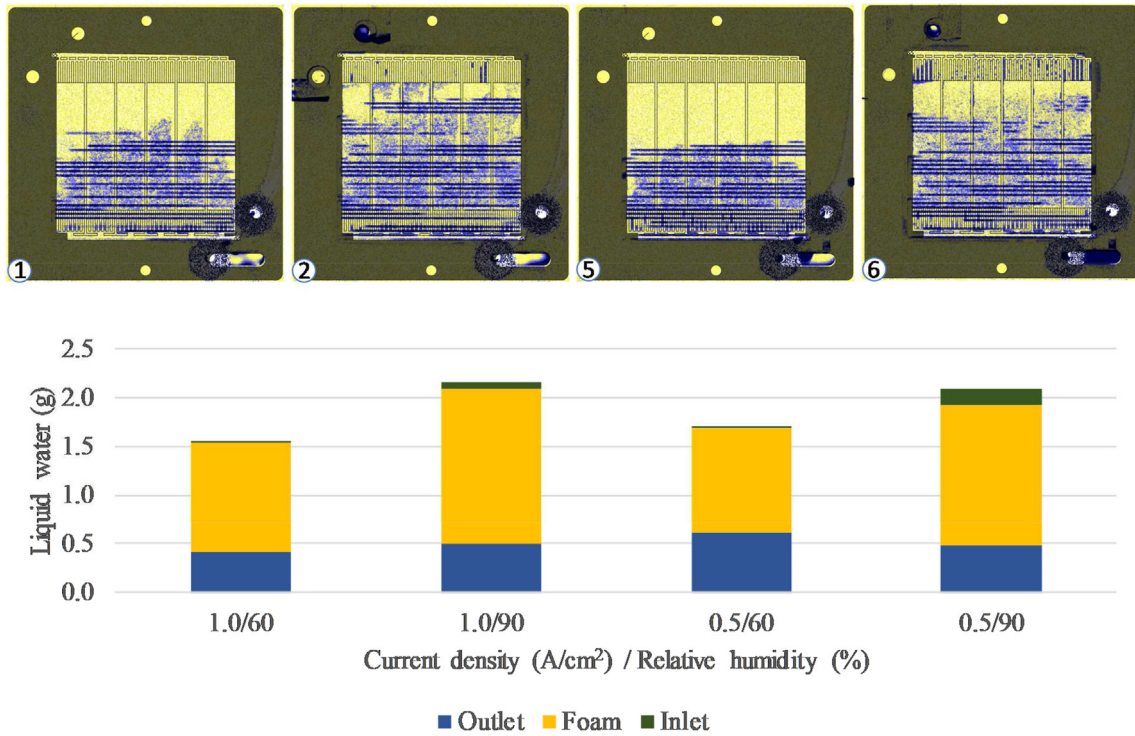
Fig. 5 – Effect of current density on water distribution (T = 65 °C, P = 0.5 bar). Liquid water distribution in the cell from neutron radiographies of the experiments 1, 2, 5 and 6 listed in Table 1 (top), and amount of water in the cell (bottom).
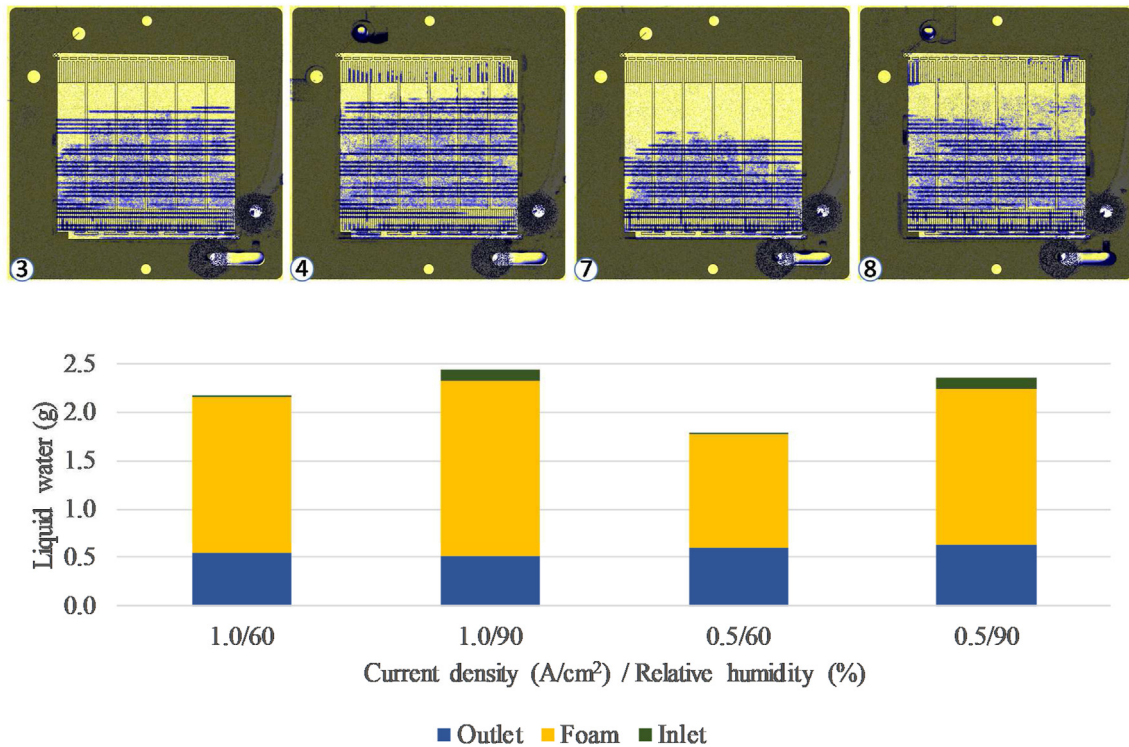

Fig. 6 – Effect of current density on water distribution (T = 65 °C, P = 1.0 bar). Liquid water distribution in the cell from neutron radiographies of the experiments 3, 4, 7 and 8 listed in Table 1 (top), and amount of water in the cell (bottom).
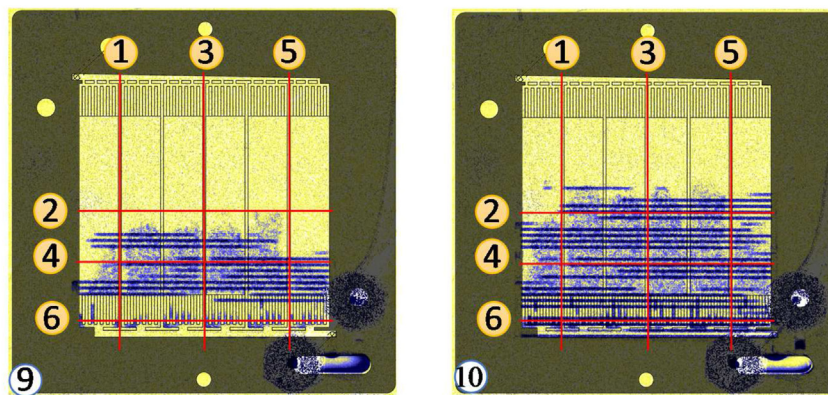
Fig. 7 – Lines draw in experiment number 9 and 10 to present the water accumulation profile in the cathode (even numbers) and the anode (odd numbers).
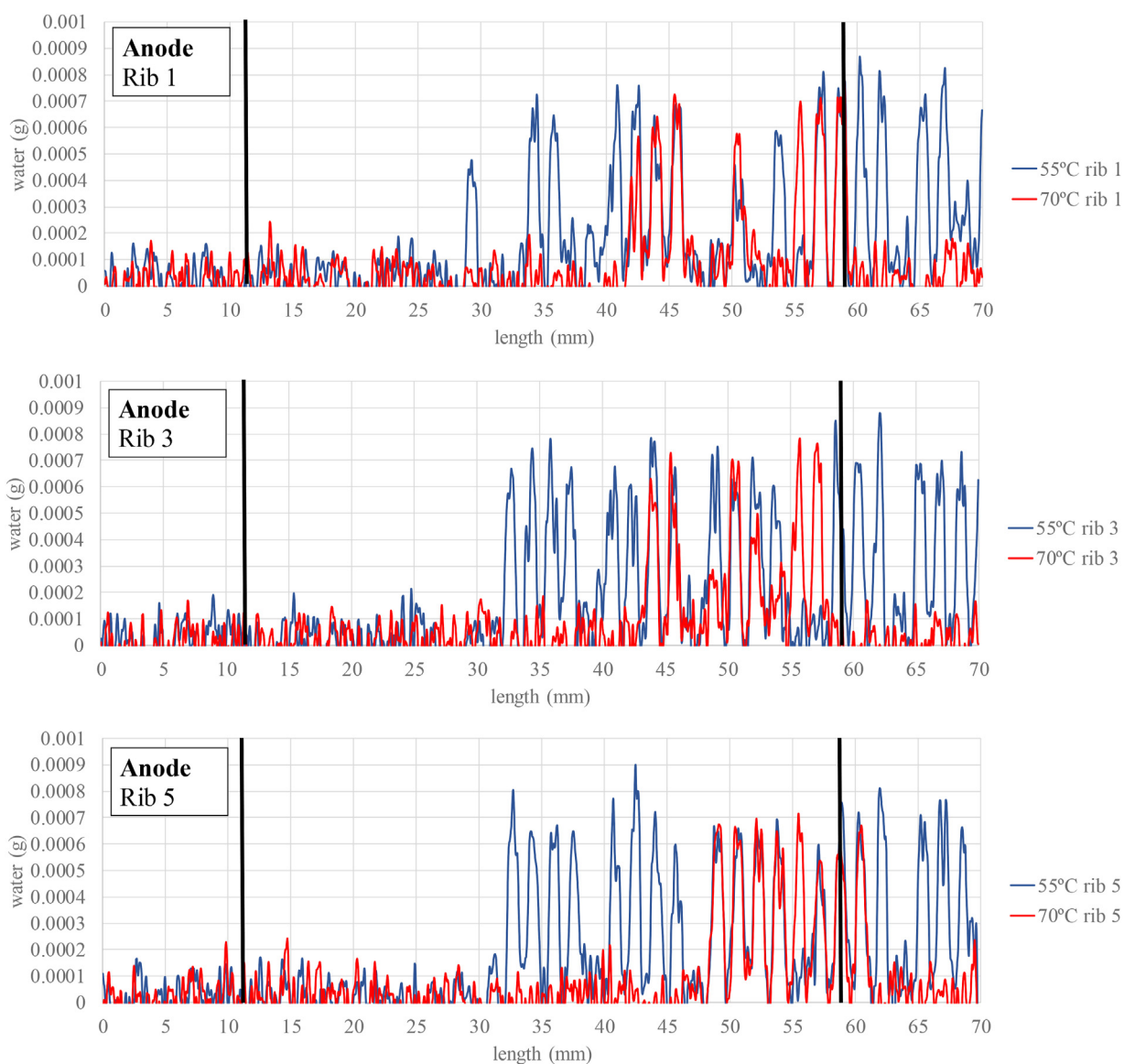

Fig. 8 – Liquid water accumulation profiles in the anode (odd lines in **Fig. 7**) for the experiments 9 and 10 listed in **Table 1**. Vertical black lines separate the three zones marked in **Fig. 1** (inlet, central and outlet).
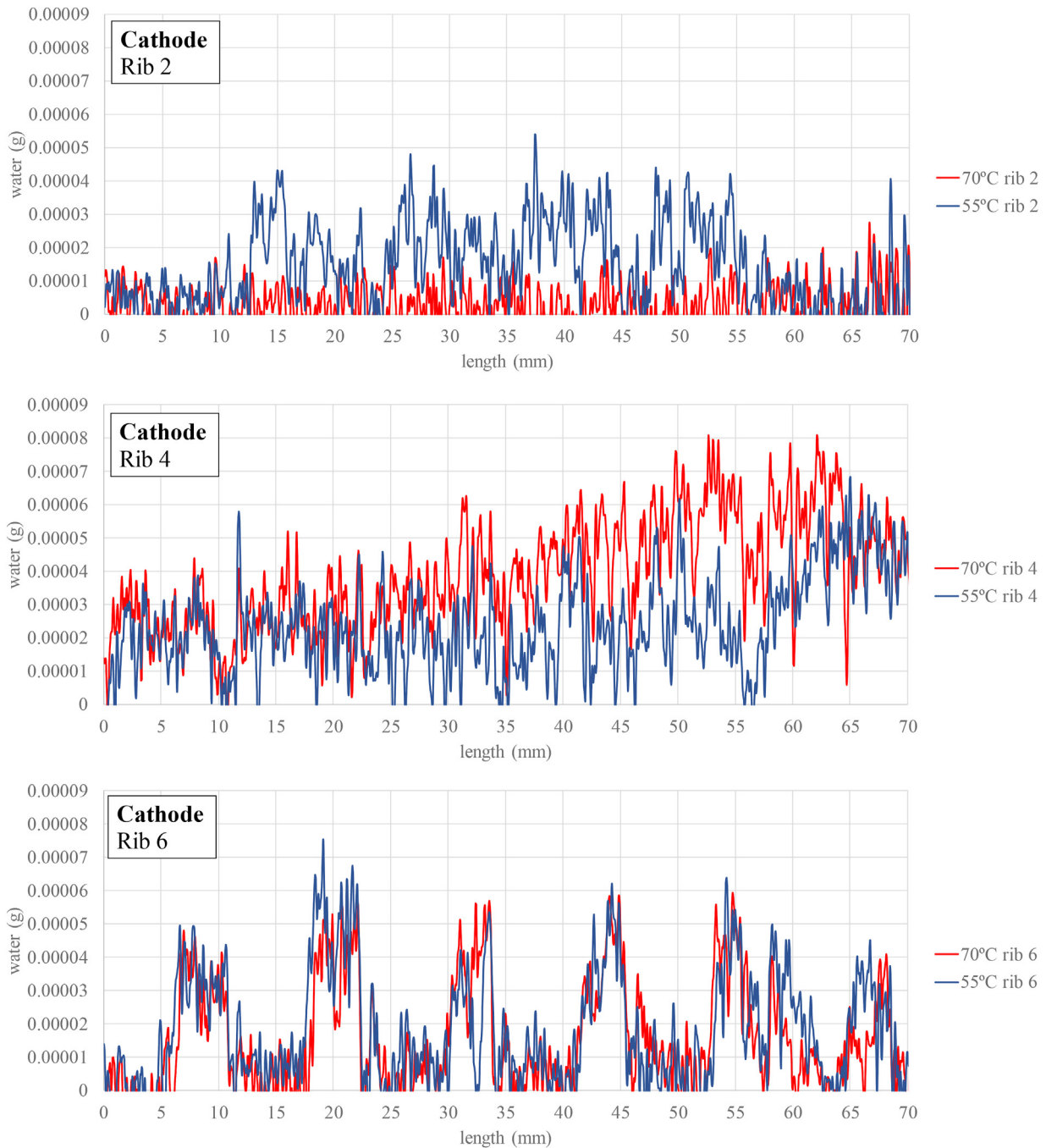
Fig. 9 – Liquid water accumulation profiles in cathode (even lines in Fig. 8) for the experiments 9 and 10 listed in Table 1.

three horizontal lines have been selected that run along three ribs of the anode flow field. Thus, the anode is isolated, and the profiles are showing only the water accumulated in the cathode side. The horizontal lines are located at the foam mid-section (line 2), foam lower section (line 4) and outlet channels section (line 6) in order to characterize the different relevant areas observed regarding the water content distributions.

In Figs. 8 and 9 the water accumulation profiles are shown. It can be observed that most of the water is present in the anode side. Focusing on the vertical distributions (along the vertical lines, Fig. 8), it can be observed how water accumulates to a greater extent in the lower half of the flow field. In the images, a clear pattern can be distinguished in the form of pointed teeth corresponding to the alternation between channels and ribs of the anode. If the test at higher temperature (red line) is compared with the one at lower temperature (blue line), it is observed that the water tends to accumulate in the anode in the part corresponding to the lower area of the cathode foams and not directly in the area closest to the gas outlet, which only begins to show a greater accumulation of

water when more than half of the cell is flooded. This fact seems to point to a transfer of water from the foam area of the cathode towards the anode through the membrane, by means of a back-diffusion mechanism. The total amount of liquid water accumulated on each one of the lines in the experiment with lower temperature is about 0.2 g, a 40% higher than the experiment at 70 °C (0.08 g).

On the other hand, the horizontal lines (Fig. 9) show the water accumulation profile in three cathode fringes. It can be seen that the water is distributed more or less homogeneously in the area of the cathode foams, however, in the lower part of the stack, a pattern in the form of plateaus is clearly seen, indicating preferential retention in certain outlet channels. As expected, a considerably larger amount of liquid water is gathered in line 2 when comparing the test at 55 °C (0.018 g) with the test at 70 °C (0.002 g) because, as aforementioned, water accumulated first closest to the gas outlet in the lower part of the cell. In line 4 and, over all, in line 6 the amount of liquid water is of the same order of magnitude. It can be seen that for line 4, the amount of liquid water presented in the experiment with a higher temperature is larger (0.05 g) than in the one at low temperature (0.03 g) indicating preference accumulation of water in this area even at high temperatures. Finally, in the line closest to the gas exit, the amount of water is quite similar for both experiments, being 0.023 g at 55 °C and 0.019 g at 70 °C.

4. Conclusions

The neutron imaging technique was used to determine liquid water content and distribution in a bioinspired design 50 cm^2 PEM fuel cell. A complete set of experiments was carried out in order to analyze the influence of the different operating conditions on the liquid water distribution. In particular, the effects of pressure, reactants relative humidity, temperature and cell current density were investigated. The amount of water in the bipolar plates was increased by high relative humidity of the inlet gas flows, high pressure, low temperatures and low current density. Similar trends were found in a previous study carried out with a parallel-serpentine design. In addition, the water accumulation profiles were draw in the anode and cathode ribs so the amount of water accumulated in each plate could be isolated. Water preferential accumulation in the anode side corresponding to the low part of the cathode foams instead of the closest area to the gases outlets points to permeation from the cathode foams to the anode.

Credit authorship contribution statement

Alfredo Iranzo: Conceptualization, Methodology, Software, Validation, Investigation, Supervision, Project Administration. **G. M. Cabello González**: Methodology, Validation, Formal Analysis, Data Curation, Visualization, Writing- Original Draft, Writing- Review & Editing. **Baltasar Toharias**: Methodology, Validation, Data Curation, **Piere Boillat**: Data Curation, Methodology, Software, Investigation. **Felipe Rosa**: Writing- Review & Editing, Supervision, Funding acquisition.

Declaration of competing interest

The authors declare that they have no known competing financial interests or personal relationships that could have appeared to influence the work reported in this paper.

Acknowledgement

REFERENCES

[1] DOE. DOE national clean hydrogen strategy and roadmap. 2022. p. 1−121.
[2] ROAD MAP TO A US Reducing emissions and driving growth across the nation [n.d].
[3] Cells F, Undertaking H. 2 J. Hydrogen roadmap Europe : a sustainable pathway for the European energy transition. Publications Office; 2019. https://doi.org/10.2843/341510.
[4] Abdelkareem MA, Elsaid K, Wilberforce T, Kamil M, Sayed ET, Olabi A. Environmental aspects of fuel cells: a review. Sci Total Environ 2021;752:141803. https://doi.org/10.1016/j.scitotenv.2020.141803.
[5] Wang G, Yu Y, Liu H, Gong C, Wen S, Wang X, et al. Progress on design and development of polymer electrolyte membrane fuel cell systems for vehicle applications: a review. Fuel Process Technol 2018;179:203−28. https://doi.org/10.1016/j.fuproc.2018.06.013.
[6] Wang Y, Ruiz Diaz DF, Chen KS, Wang Z, Adroher XC. Materials, technological status, and fundamentals of PEM fuel cells − a review. Mater Today 2020;32:178−203. https://doi.org/10.1016/j.mattod.2019.06.005.
[7] Liu Q, Lan F, Chen J, Zeng C, Wang J. A review of proton exchange membrane fuel cell water management: membrane electrode assembly. J Power Sources 2022;517:230723. https://doi.org/10.1016/j.jpowsour.2021.230723.
[8] Vichard L, Steiner NY, Zerhouni N, Hissel D. Hybrid fuel cell system degradation modeling methods: a comprehensive review. J Power Sources 2021;506:230071. https://doi.org/10.1016/j.jpowsour.2021.230071.
[9] Okonkwo PC, Otor C. A review of gas diffusion layer properties and water management in proton exchange membrane fuel cell system. Int J Energy Res 2021;45:3780−800. https://doi.org/10.1002/er.6227.
[10] Zhang G, Jiao K. Multi-phase models for water and thermal management of proton exchange membrane fuel cell: a review. J Power Sources 2018;391:120−33. https://doi.org/10.1016/j.jpowsour.2018.04.071.
[11] Andersson M, Mularczyk A, Lamibrac A, Beale SB, Eller J, Lehnert W, et al. Modeling and synchrotron imaging of droplet detachment in gas channels of polymer electrolyte

fuel cells. J Power Sources 2018;404:159—71. https://doi.org/10.1016/j.jpowsour.2018.10.021.

[12] Iranzo A, Boillat P, Oberholzer P, Guerra J. A novel approach coupling neutron imaging and numerical modelling for the analysis of the impact of water on fuel cell performance. Energy 2014;68:971—81. https://doi.org/10.1016/j.energy.2014.03.014.

[13] Zhao J, Tu Z, Chan SH. In-situ measurement of humidity distribution and its effect on the performance of a proton exchange membrane fuel cell. Energy 2022;239:122270. https://doi.org/10.1016/j.energy.2021.122270.

[14] Jiao K, Li X. Water transport in polymer electrolyte membrane fuel cells. Prog Energy Combust Sci 2011;37:221—91. https://doi.org/10.1016/j.pecs.2010.06.002.

[15] Kim S-G, Lee S-J. A review on experimental evaluation of water management in a polymer electrolyte fuel cell using X-ray imaging technique. J Power Sources 2013;230:101—8. https://doi.org/10.1016/j.jpowsour.2012.12.030.

[16] Iranzo A, Boillat P. Liquid water distribution patterns featuring back-diffusion transport in a PEM fuel cell with neutron imaging. Int J Hydrogen Energy 2014;39:17240—5. https://doi.org/10.1016/j.ijhydene.2014.08.042.

[17] Iranzo A, Boillat P, Biesdorf J, Tapia E, Salva A, Guerra J. Liquid water preferential accumulation in channels of PEM fuel cells with multiple serpentine flow fields. Int J Hydrogen Energy 2014;39:15687—95. https://doi.org/10.1016/j.ijhydene.2014.07.101.

[18] Iranzo A, Boillat P, Rosa F. Validation of a three dimensional PEM fuel cell CFD model using local liquid water distributions measured with neutron imaging. Int J Hydrogen Energy 2014;39:7089—99. https://doi.org/10.1016/j.ijhydene.2014.02.115.

[19] Kardjilov N, Manke I, Woracek R, Hilger A, Banhart J. Advances in neutron imaging. Mater Today 2018;21:652—72. https://doi.org/10.1016/j.mattod.2018.03.001.

[20] Martinez N, Porcar L, Escribano S, Micoud F, Rosini S, Tengattini A, et al. Combined operando high resolution SANS and neutron imaging reveals in-situ local water distribution in an operating fuel cell. ACS Appl Energy Mater 2019;2:8425—33. https://doi.org/10.1021/acsaem.9b01266.

[21] Iranzo A, Gregorio JM, Boillat P, Rosa F. Bipolar plate research using Computational Fluid Dynamics and neutron radiography for proton exchange membrane fuel cells. Int J Hydrogen Energy 2020;45:12432—42. https://doi.org/10.1016/j.ijhydene.2020.02.183.

[22] Iranzo A, Boillat P, Biesdorf J, Salva A. Investigation of the liquid water distributions in a 50cm2 PEM fuel cell: effects of reactants relative humidity, current density, and cathode stoichiometry. Energy 2015;82:914—21. https://doi.org/10.1016/j.energy.2015.01.101.

[23] Iranzo A, Arredondo CH, Kannan AM, Rosa F. Biomimetic flow fields for proton exchange membrane fuel cells: a review of design trends. Energy 2020;190:116435. https://doi.org/10.1016/j.energy.2019.116435.

[24] Zhang S, Xu H, Qu Z, Liu S, Talkhoncheh FK. Bio-inspired flow channel designs for proton exchange membrane fuel cells: a review. J Power Sources 2022;522:231003. https://doi.org/10.1016/j.jpowsour.2022.231003.

[25] Ozden A, Ercelik M, Ouellette D, Colpan CO, Ganjehsarabi H, Hamdullahpur F. Designing, modeling and performance investigation of bio-inspired flow field based DMFCs. Int J Hydrogen Energy 2017;42:21546—58. https://doi.org/10.1016/j.ijhydene.2017.01.007.

[26] Karthikeyan M, Karthikeyan P, Muthukumar M, Magesh Kannan V, Thanarajan K, Maiyalagan T, et al. Adoption of novel porous inserts in the flow channel of pem fuel cell for the mitigation of cathodic flooding. Int J Hydrogen Energy 2020;45:7863—72. https://doi.org/10.1016/j.ijhydene.2019.08.151.

[27] Marappan M, Narayanan R, Manoharan K, Vijayakrishnan MK, Palaniswamy K, Karazhanov S, et al. Scaling up studies on PEMFC using a modified serpentine flow field incorporating porous sponge inserts to observe water molecules. Molecules 2021;26. https://doi.org/10.3390/molecules26020286.

[28] Kermani MJ, Moein-Jahromi M, Hasheminasab MR, Ebrahimi F, Wei L, Guo J, et al. Application of a foam-based functionally graded porous material flow-distributor to PEM fuel cells. Energy 2022;254:124230. https://doi.org/10.1016/j.energy.2022.124230.

[29] Chen T, Liu S, Yang L. Development of flow field plates based on asymmetric leaf structure for PEM fuel cells. Int J Mater Struct Integr 2017;11:229—43. https://doi.org/10.1504/IJMSI.2017.089657.

[30] Kahraman H, Coban A. Performance improvement of a single PEM fuel cell using an innovative flow field design methodology. Arabian J Sci Eng 2020;45:5143—52. https://doi.org/10.1007/s13369-020-04368-y.

[31] Kang HC, Jum KM, Sohn YJ. Performance of unit PEM fuel cells with a leaf-vein-simulating flow field-patterned bipolar plate. Int J Hydrogen Energy 2019;44:24036—42. https://doi.org/10.1016/j.ijhydene.2019.07.120.

[32] Nasu M, Yanai H, Hirayama N, Adachi H, Kakizawa Y, Shirase Y, et al. Neutron imaging of generated water inside polymer electrolyte fuel cell using newly-developed gas diffusion layer with gas flow channels during power generation. J Power Sources 2022;530:231251. https://doi.org/10.1016/j.jpowsour.2022.231251.

[33] Asadzade M, Shamloo A. Design and simulation of a novel bipolar plate based on lung-shaped bio-inspired flow pattern for PEM fuel cell. Int J Energy Res 2017;41:1730—9. https://doi.org/10.1002/er.3741.

[34] Trogadas P, Cho JIS, Neville TP, Marquis J, Wu B, Brett DJL, et al. A lung-inspired approach to scalable and robust fuel cell design. Energy Environ Sci 2018;11:136—43. https://doi.org/10.1039/c7ee02161e.

[35] Bethapudi VS, Hack J, Trogadas P, Cho JIS, Rasha L, Hinds G, et al. A lung-inspired printed circuit board polymer electrolyte fuel cell. Energy Convers Manag 2019;202:112198. https://doi.org/10.1016/j.enconman.2019.112198.

[36] Cho JIS, Neville TP, Trogadas P, Meyer Q, Wu Y, Ziesche R, et al. Visualization of liquid water in a lung-inspired flow-field based polymer electrolyte membrane fuel cell via neutron radiography. Energy 2019;170:14—21. https://doi.org/10.1016/j.energy.2018.12.143.

[37] Cho JIS, Neville T, Trogadas P, Wu B, Brett D, Coppens MO. Nature-inspired flow-fields and water management for PEM fuel cells. Fuels Petrochemicals Div 2018 - Core Program Area 2018 AIChE Annu Meet 2018:74—5. https://doi.org/10.1149/ma2020-02332171mtgabs.

[38] Suárez C, Iranzo A, Toharias B, Rosa F. Experimental and numerical Investigation on the design of a bioinspired PEM fuel cell. Energy 2022:124799. https://doi.org/10.1016/j.energy.2022.124799.

[39] Jiao K, Xuan J, Du Q, Bao Z, Xie B, Wang B, et al. Designing the next generation of proton-exchange membrane fuel cells. Nature 2021;595:361—9. https://doi.org/10.1038/s41586-021-03482-7.

[40] Taherian F, Marcon V, van der Vegt NFA, Leroy F. What is the contact angle of water on graphene? Langmuir 2013;29:1457—65. https://doi.org/10.1021/la304645w.

[41] Belyaeva LA, Tang C, Juurlink L, Schneider GF. Macroscopic and microscopic wettability of graphene. Langmuir 2021;37:4049—55. https://doi.org/10.1021/acs.langmuir.0c02817.

[42] Kumar A, Reddy RG. Materials and design development for bipolar/end plates in fuel cells. J Power Sources 2004;129:62–7. https://doi.org/10.1016/j.jpowsour.2003.11.011.

[43] Wu Y, Cho JIS, Whiteley M, Rasha L, Neville TP, Ziesche R, et al. Characterization of water management in metal foam flow-field based polymer electrolyte fuel cells using in-operando neutron radiography. Int J Hydrogen Energy 2020;45:2195–205. https://doi.org/10.1016/j.ijhydene.2019.11.069.

[44] Tseng C-J, Tsai BT, Liu Z-S, Cheng T-C, Chang W-C, Lo S-K. A PEM fuel cell with metal foam as flow distributor. Energy Convers Manag 2012;62:14–21. https://doi.org/10.1016/j.enconman.2012.03.018.

[45] Chen Z, Ren W, Gao L, Liu B, Pei S, Cheng H-M. Three-dimensional flexible and conductive interconnected graphene networks grown by chemical vapour deposition. Nat Mater 2011;10:424–8. https://doi.org/10.1038/nmat3001.

[46] Park JE, Lim J, Kim S, Choi I, Ahn C-Y, Hwang W, et al. Enhancement of mass transport in fuel cells using three-dimensional graphene foam as flow field. Electrochim Acta 2018;265:488–96. https://doi.org/10.1016/j.electacta.2018.01.191.

[47] Park JE, Lim J, Lim MS, Kim S, Kim O-H, Lee DW, et al. Gas diffusion layer/flow-field unified membrane-electrode assembly in fuel cell using graphene foam. Electrochim Acta 2019;323:134808. https://doi.org/10.1016/j.electacta.2019.134808.

[48] Owejan JP, Gagliardo JJ, Falta SR, Trabold TA. Accumulation and removal of liquid water in proton exchange membrane fuel cells. J Electrochem Soc 2009;156:B1475. https://doi.org/10.1149/1.3242295.

[49] Boillat P, Iranzo A, Biesdorf J. Layer by layer segmentation of water distribution from neutron imaging of large scale cells. J Electrochem Soc 2015;162:F531–6. https://doi.org/10.1149/2.0511506jes.